An Anatomy Aware Hybrid Deep Learning Framework for Lung Cancer Tumor Stage Classification

Saniah Kayenat Chowdhury[1], Rusab Sarmun[2], Muhammad E. H. Chowdhury[3*], Sohaib Bassam Zoghoul[4], Israa Al-Hashimi[5], Adam Mushtak[6], Amith Khandakar[7]

[1]Department of Robotics and Mechatronics Engineering, University of Dhaka, Bangladesh. Email: kayenat945@gmail.com (SKC)

[2]Department of Electrical and Electronics Engineering, University of Dhaka, Bangladesh. Email: rusabsarmun@gmail.com (RS)

[3,7]Department of Electrical Engineering, College of Engineering, Qatar University, Doha 2713, Qatar. Email: mchowdhury@qu.edu.qa (MEHC), amitk@qu.edu.qa (AK)

[4,5]Department of Radiology, Hamad Medical Corporation, Doha, Qatar. Email: sohaibzoghoul@gmail.com (SBZ), Ialhashimi@hamad.qa (IAH), adamrads94@gmail.com (AM)

[6]Department of Biomedical Technology, College of Applied Medical Sciences in Al-Kharj, Prince Sattam Bin Abdulaziz University, Al-Kharj 11942, Saudi Arabia. Email: ama.alqahtani@psau.edu.sa (AA)

*Correspondence: Muhammad E.H. Chowdhury (mchowdhury@qu.edu.qa).

Abstract

Accurate lung cancer tumor staging is crucial for prognosis and treatment planning. However, it remains challenging for end-to-end deep learning approaches, as such approaches often overlook spatial and anatomical information that are central to the tumor-node-metastasis system. The tumor stage depends on multiple quantitative criteria, including the tumor size and its proximity to nearest anatomical structures, and small variations can alter the staging outcome. We propose a medically grounded hybrid pipeline that performs staging by explicitly measuring the tumor's size and distance properties rather than treating it as a pure image classification task. Our method employs specialized encoder–decoder networks to precisely segment the lung and adjacent anatomy, including the lobes, tumor, mediastinum, and diaphragm. Subsequently, we extract the necessary tumor properties i.e. measure the largest tumor dimension and calculate the distance between the tumor and neighboring anatomical structures by a quantitative analysis of the segmentation masks. Finally, we apply rule-based tumor staging aligned with the medical guidelines. This novel framework has been evaluated on the Lung-PET-CT-Dx dataset, demonstrating superior performance compared to traditional deep learning models, achieving an overall classification accuracy of 91.36%. We report the per-stage F1-scores of 0.93 (T1), 0.89 (T2), 0.96 (T3), and 0.90 (T4), a critical evaluation aspect often omitted in prior literature. To our knowledge, this is the first study that embeds explicit clinical context into tumor stage classification. Unlike standard convolutional neural networks that operate on an uninterpretable 'black box' manner, our method offers both state-of-the-art performance and transparent decision support.

Keywords: Lung Cancer, Tumor Stage Classification, Medical Image Segmentation, Deep Learning, Computed Tomography Imaging, Anatomical Aware Framework

1. Introduction

Artificial Intelligence has revolutionized medical diagnosis and prognosis, providing AI-driven systems capable of delivering outcomes comparable to expert clinicians [1], [2], [3]. In oncology, especially, deep learning methods have demonstrated remarkable potential for early cancer detection, precise disease classification, and improved treatment strategies [4], [5], [6]. Lung cancer, in particular, remains a major global health concern and one of the deadliest diseases worldwide [7]. A study of 2024 by Zhou et al. shows that it ranks as the leading cause of cancer-related deaths and approximately 2.48 million new cases are reported every year [8]. It is the most frequently occurring malignancy in men and the second most commonly diagnosed cancer in women [7]. Therefore, early detection and accurate classification of lung cancer are crucial to improve survival rates for patients [9], [10]. Lung cancer classification primarily follows the Tumor-Node-Metastasis (TNM) staging system, which divides cancer classification into three primary categories [11]:

- **T-stage**: Describes the size and extent of the primary tumor.
- **N-stage**: Tells whether cancer has spread to nearby lymph nodes.
- **M-stage**: Indicates whether cancer has metastasized to distant body parts.

Precise staging of lung cancer is essential for assessing the tumor's extent and guiding clinical decision-making. The Tumor Stage (T-stage) is the first staging to be done, and it categorizes tumors into four main classes: T1 (tumor size ≤3 cm), T2 (tumor >3 cm but ≤5 cm), T3 (tumor >5 cm but ≤7 cm), and T4 (tumor >7 cm) [11], [12], [13]. However, T-stage determination is not limited to tumor size alone; it also depends on tumor location, and involvement with surrounding anatomical structures such as the mediastinum, thoracic cavity, carina, diaphragm etc. Moreover, whether the tumor is surrounded only by lung tissue or is nearing the lung walls is a crucial consideration. Thus, the tumor staging becomes an extremely complex clinical task.
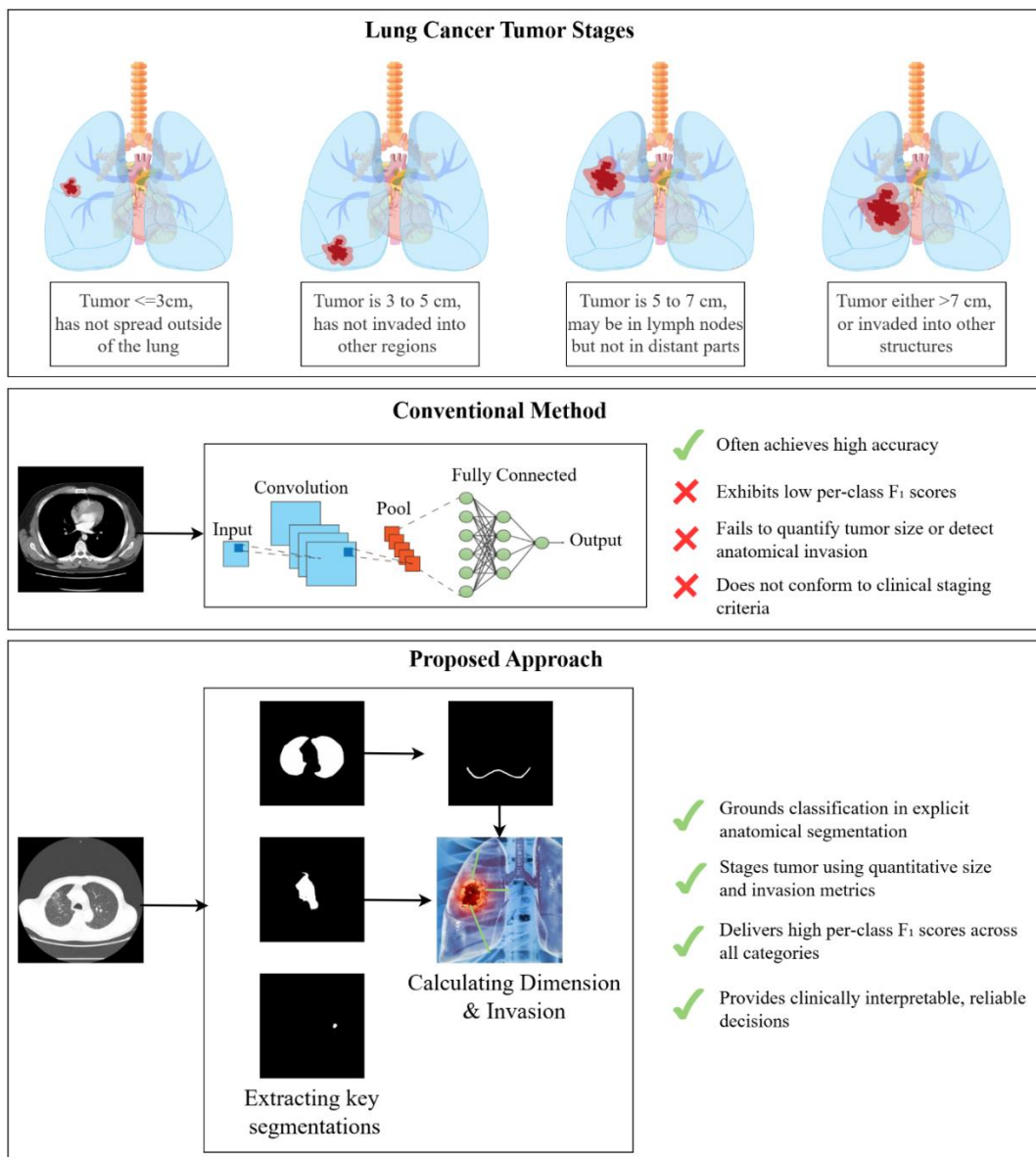
Figure 1.1 Comparing conventional CNN approaches and proposed segmentation-based pipeline for lung cancer tumor staging, emphasizing on the importance of calculating tumor properties for clinical T-staging.

Currently, medical imaging techniques such as Computed Tomography (CT), Positron Emission Tomography (PET), and PET/CT scans are commonly used by experts to diagnose and classify lung cancer, providing detailed anatomical and metabolic information [9], [14]. However, during staging, clinicians often face limitations in accurately capturing the complex anatomical relationships between the tumor and surrounding structures, leading to potential misclassification. Additionally, the reliance on manual interpretation introduces variability and can be time-consuming. These challenges highlight the need for automation through deep learning methods in order to streamline and enhance the classification process. Existing deep learning approaches for T-stage classification face extreme challenges. Many of these methods treat staging as a pure image classification problem, relying on conventional classifiers to output a stage label. Figure 1.1 illustrates this approach, highlighting its limitations. This approach has fundamental limitations. A pure Convolutional Neural Network (CNN) tnbased classifier does not explicitly explore the anatomical context and quantitative criteria that are essential for T-staging. For example, according to the International Association for the Study of Lung Cancer (IASLC) guidelines, a tumor with the largest dimension of 6cm is generally labeled as a T3 stage. However, if there is any invasion with mediastinum, diaphragm, esophagus, vertebral body, carina etc., the T-stage is classified as T4 regardless of its size [12]. These conditions are explicitly defined in the IASLC guidelines (described in Section 3.9), but a generic CNN may struggle with such fine-grained distinctions, failing to recognize multiple organs and the distances between them from a single input [15], [16]. Furthermore, CNN-based classification models offer limited interpretability regarding their decision-making criteria, reducing their trustworthiness for borderline cases. Motivated by these limitations, we propose reframing tumor staging as a localization and measurement problem, rather than solely a classification task. This involves distinct segmentation networks tailored for segmenting key regions, including the lungs, mediastinum, diaphragm, and tumor. By explicitly extracting clinically relevant tumor properties (its size, distance to and invasion of adjacent structures) utilizing these segmentation masks, our method directly adheres to IASLC-defined criteria for T-stage determination. This approach moves beyond end-to-end CNN classifiers and provides an interpretable, reproducible staging pipeline that is clinically relevant. The results achieved via our system highlight the potential of our approach to accurately classify lung cancer T-stage, which could significantly impact clinical decision-making and treatment planning. The comparison in performance between conventional CNN methods and our proposed framework in Section 5.3 further clarifies the need to incorporate medical context to T-staging.

2. Literature Review

This section provides a comprehensive review of existing literature pertinent to deep learning-based classification of lung cancer and T-staging. Initially, we discuss prior works focused broadly on classification of lung cancer subtypes. Subsequently, we narrow the scope specifically to the literature related to T-stage classification, emphasizing the necessity and potential impact of our proposed segmentation-driven staging framework.

2.1 Lung Cancer and Nodule Classification

The application of CNNs has demonstrated remarkable success in various aspects of lung cancer analysis, particularly in the classification of pulmonary nodules. Multiple studies have shown the potential of CNN-based models to accurately distinguish between normal and nodular lung tissue on CT scans [17],[18]. Moreover, the classification among lung cancer classes has also witnessed massive success in detecting cancer classes such as - ADC, SCLC, SCC, and LCC cancer types [19], [20],[21]. Khan et al. proposed a VGG-19 [22] based scheme for both segmentation and classification of lung nodules, achieving a high classification accuracy on two popular lung tumor datasets [23] and [24]. Their use of combining deep features with hand crafted features benefitted the overall performance of the network. Beyond this, deep learning has also proven to be exceptionally useful to the classification of lung cancer subtypes. Wehbe et al. [25] utilized a very popular detection model YOLOv8 (You Only Look Once) [26] for lung cancer subtype classification, achieving a mean Average Precision (mAP) score of 96.8% at IoU = 0.5. Similarly, Barbouchi et al. [21] adopted a Detection Transformer (DeTr) [27] model for lung cancer detection and histologic classification using integrated PET/CT images. It results in a mean IOU of 83% in the testing data. Additionally, the classification results of this work also show remarkable numbers, providing an F1-score of 93.66%. This works are testament to the success of using deep learning in the classification of lung cancer classes.

2.2 T-Stage Classification

While deep learning has excelled in classification tasks, achieving precise T-staging based on these spatial criteria remains a significant challenge and an area of research still relatively unexplored. Barbouchi et al.'s DeTr transformer [21] aimed to predict both T-staging and histologic classification using PET/CT images, classifying T-stages into T1, T2, and T3/T4. The term 'T3/T4' indicates that this work could not differentiate between T-stage 3 and 4. This work reports a high overall F-1 score (95.63%) without highlighting class specific performances. Moreover, the extent to which the model explicitly analyses tumor localization and invasion for T-staging is not detailed. The authors also note that their work aims to bring together tumor localization and staging within a single model, leveraging the attention mechanism of the transformer to establish relationships between pixel features. Another work by Sathiyamurthy et al. [28] proposed an automated technique for lung cancer T-stage detection and classification using an improved U-Net model with an Advanced Residual Network (ARESNET). Their method involves automated lung nodule mask generation and utilizes an extended mobius augmentation technique for data balancing, and achieves an overall accuracy of 94% across all the classes. This approach incorporates segmentation, suggesting a reliance on tumor size derived from the segmented mask, but the explicit analysis of localization and invasion is not thoroughly described. Again, this research lacks a more reliable performance metrics such as F1-score and fails to deliver class wise performance. More research to classify T-staging has been done in [29], [25],[30], all having one thing in common – depending solely on traditional CNN models to output a class of T-stage, without taking the size or location of the tumor in consideration. Therefore, the question of whether the studies are in accordance to the clinical approach of staging decision remain unsolved. The absence of extensive performance breakdown for each stage class further indicates the necessity for more work. While some studies report high accuracies in T-stage classification, the methodologies often lack explicit details on how the models analyze the spatial relationships critical for determining the T parameter according to the TNM system.

Recognizing the challenges of current deep learning models in T-stage classification, this research argues for the critical incorporation of the discussed clinically relevant tumor properties. By developing a model

that is sensitive to both the visual patterns within the tumor and its specific location and size relative to key anatomical structures, we aim to create a more clinically meaningful and accurate T-stage classification system. The following are the major contributions that have been presented in our study:

• Design and implementation of three dedicated segmentation networks – LungNet, MediNet, and TumorNet for accurate segmentation of the lung, mediastinum, and tumor, respectively.

• Applying the trained segmentation networks on the Lung-PET-CT-Dx dataset [23] as external validation set to generate precise ground truth segmentation masks of the regions.

• Extracting crucial tumor properties: its largest dimension, spatial relationship to the anatomical structures, and potential invasion - using a unique contour-based distance computation method.

• Implementing a novel automated pipeline for T-stage classification of lung cancer patients based on extracted tumor properties, aligned with IASLC guidelines.

The following sections are structured into five cohesive parts. Section 3 offers a deep dive into the models implemented, and the full detail of our experimental methodology. Section 4 and 5 demonstrates the experimental setup and reveals the study's results, presenting a comprehensive analysis of model performance. This section also sheds light on the limitations and future work prospects of this study. The paper culminates in this Section 6, offering concluding remarks and insights.

3. Methodology

The proposed methodology for this research involves a multi-stage pipeline designed to classify the T-stage of lung cancer patients, as illustrated in Figure 3.1. In the initial stage, we collect and pre-process all the datasets incorporated in this study. This is followed by data augmentation and train-test splits. There are three separate and unique Encoder-Decoder (E-D) CNN architectures designed and trained in this work, namely:

1. **LungNet** – performs segmentation of the lungs.
2. **MediNet** – is dedicated to segmenting the mediastinum.
3. **TumorNet** – generates precise segmentation masks for the lung tumor.

The three models are collectively referred to as AnatomicalNets. The primary objective is to obtain the segmentation masks and utilize them to extract the necessary tumor properties for T-stage classification. However, the primary dataset, Lung PET-CT-Dx [23] does not inherently include ground truth masks, providing only bounding box annotations for lung tumors. To resolve this limitation, we train the AnatomicalNets on multiple publicly available datasets [24, 31-35], each of which possesses high-quality ground truth masks. Following this, these models are applied to the Lung-Pet-CT-Dx dataset to generate the ground truth segmentation masks. Additionally, a dedicated detection model is trained on the primary dataset to precisely localize lung tumors within CT slices. Region of interest (ROI) identified by this detection model are cropped from CT images when they are used as external validation set in the TumorNet. A detection followed by segmentation approach makes sure that all the redundant information is eliminated and the model only focuses on the region that's important. All the networks within AnatomicalNets achieves high dice similarity scores, ensuring reliability and robustness of the generated masks. The last step of the initial stage evaluating the tumor's proximity to the diaphragm. For that, a contour-based distance estimation technique is applied. This completes the first stage of the multi-stage pipeline.

In the second stage, the tumor properties required for T-staging are obtained. The properties evaluated in this study are:

1. Tumor size or the largest tumor dimension.
2. Distance between tumor and lung walls.
3. Distance between tumor and mediastinum.
4. Distance between tumor and diaphragm.

These properties are calculated using the primary dataset's generated segmentation masks. The distance is quantified by measuring the maximum difference between the contours of the respective masks. To obtain

the tumor size, maximum distance between the contour points of the tumor mask is evaluated. This completes the first two phases of the pipeline, effectively localizing the tumor and providing quantitative measures.

In the third and final stage, we leverage the obtained tumor properties and perform automated T-stage classification according to the IASLC conditions [12]. The tumor properties provide information on the tumor size and whether its invading other key structures, and T-stage guidelines are based on such criteria. The following sections of the paper further detail the data acquisition and preprocessing strategies, model architecture specifics, and procedures for extracting tumor properties.
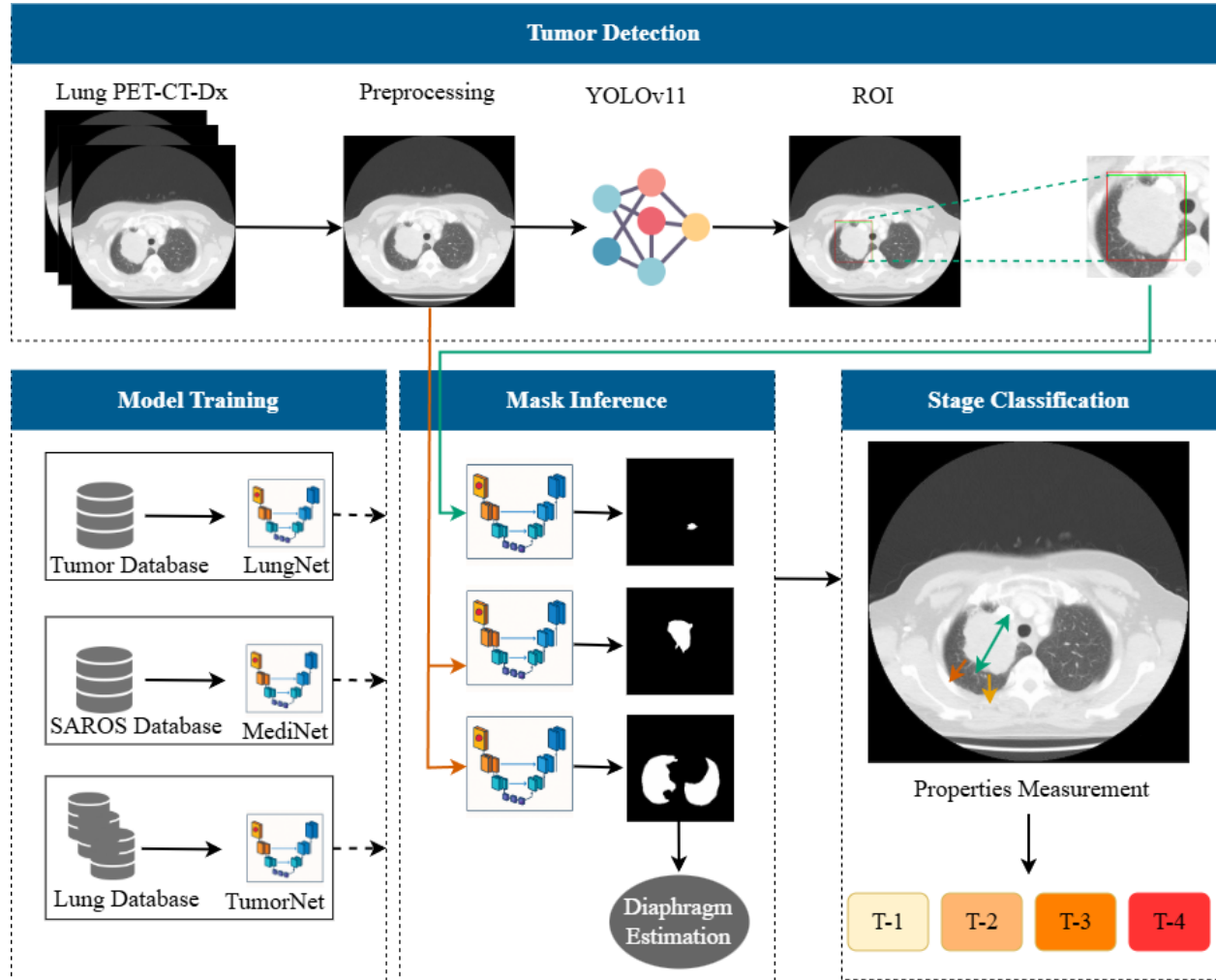

Figure 3.1 Overview of the proposed methodology. The tumor detection module is trained on the Lung PET-CT-Dx dataset to localize the tumor region. Corresponding databases are used to train the AnatomicalNets. During inference, either the full CT image or the detected ROI is used as input to generate segmentation masks. The Diaphragm position is estimated from lung segmentation masks. Final T-staging is performed based on the tumor properties extracted. T-staging: T1 (≤3 cm and surrounded by lung tissue), T2 (>3 cm but ≤5 cm), T3 (>5 cm but ≤7 cm), and T4 (>7 cm or invasion into critical structures).

3.1 Datasets Acquisition

This study uses Lung PET-CT-Dx Dataset [23] for T-stage classification among lung cancer patients. This dataset contains 355 subjects with CT, PET, and PET-CT scans. Among them, 220 patients include individual CT scans; totaling 31,717 CT slices, each annotated with a bounding box for lung tumors. Patients are classified into four lung cancer types: Adenocarcinoma, Small Cell Carcinoma, Large Cell Carcinoma, and Squamous Cell Carcinoma. However, our work focuses specifically on classifying the T-stage, with diagnoses falling into one of the following stages: T1 (49 patients), T2 (42 patients), T3 (34 patients), or T4 (95 patients). These labels were not directly usable from the original dataset. Upon reviewing the provided ground truth labels, three expert radiologists independently re-evaluated and re-annotated the T-stage classifications, as discrepancies were observed in the original annotations that did not align with clinical imaging features. This dataset, hereafter referred to as the primary dataset, does not provide any ground truth segmentation masks for the lung and adjacent regions. Therefore, in order to generate segmentation masks, we use this dataset as an external validation set on the proposed segmentation networks. To generate segmentation mask for the lung, we train LungNet on three datasets collectively referred to as the lung database. The first dataset [33] includes 20 labeled COVID-19 CT scans that results in 3520 individual slices with ground truth lung masks. The second dataset [32] contains 9 patients and 829 CT slices with ground truth lung masks created by expert radiologists. The final dataset [35] for the lung segmentation is a popular dataset sourced from Kaggle with 267 CT slices and their corresponding lung masks. Together, these datasets provide a total of 4,616 CT slices. The tumor database consists of one dataset: the Medical Segmentation Decathlon (MSD) [31] dataset, comprising 64 CT volumes and among them, 1224 CT slices have ground truth tumor segmentation masks generated by experts. Finally, the MediNet is trained on the SAROS database, which is a dataset for whole-body region and organ segmentation in CT imaging named SAROS dataset [34]. The SAROS dataset is a collection of 725 patients, with a total of 5,513 CT images annotated for 13 body regions and 6 body parts, including the mediastinum. This research is able to generate segmentation masks for the primary dataset [23] using multiple datasets and the large number of collected data ensures the efficacy and reliability of the masks. A summarization of the secondary and primary datasets is shown in Table 1.

Table 1 Summary of the datasets utilized in this research

			Availability of Ground Truth Masks		
Dataset	**Number of Patients**	**Number of CT Slices**	**Lung**	**Tumor**	**Mediastinum**
Lung PET-CT-Dx Dataset	220	31,717			
COVID-19 CT lung and infection segmentation dataset	20	3520	✓		
COVID-19 CT segmentation dataset	9	829	✓		
Finding and Measuring Lungs in CT Data	N\A	267	✓		

Medical Segmentation Decathlon (MSD)	64	1224		✓	
SAROS	725	5513			✓

3.2 Data Pre-Processing

All CT images in the primary and secondary datasets are provided in DICOM format, except for the CT studies provided in SAROS database [34], which are in Neuroimaging Informatics Technology Initiative (NIfTI) format. The CT scans span a vast range of window levels, labeled in Hounsfield Units (HU). All the CT slices are set to the lung window (window width: 1400 HU, window center: -700 HU), and converted into Portable Network Graphics (PNG) format images. The image intensities have been normalized and mapped to pixel values in the range of 0-255. To ensure consistency across datasets, the intensity interval is adjusted for each dataset, thereby creating uniform image content. All PNG images are subsequently resized to 256x256 pixels for segmentation and detection networks. A key image enhancement technique, Contrast-Limited Adaptive Histogram Equalization (CLAHE), is applied to all images. CLAHE enhances soft-tissue contrast by locally redistributing pixel intensities without amplifying noise. For this study, the CLAHE parameters used are clipLimit = 1.0 and tileGridSize = (16,16). It is important to note that the tumor database [31], includes one additional pre-processing step. To create highly accurate tumor segmentation masks, the ground truth masks are superimposed on the CT to extract a rectangular region enclosing the tumor. Padding is applied for convenience, and the resulting region is cropped from the CT slice, then resized to 256x256 pixels before being passed to the tumor segmentation network. This approach has been exceptionally beneficial for tumor segmentation where it is imperative to capture even the smallest detail.
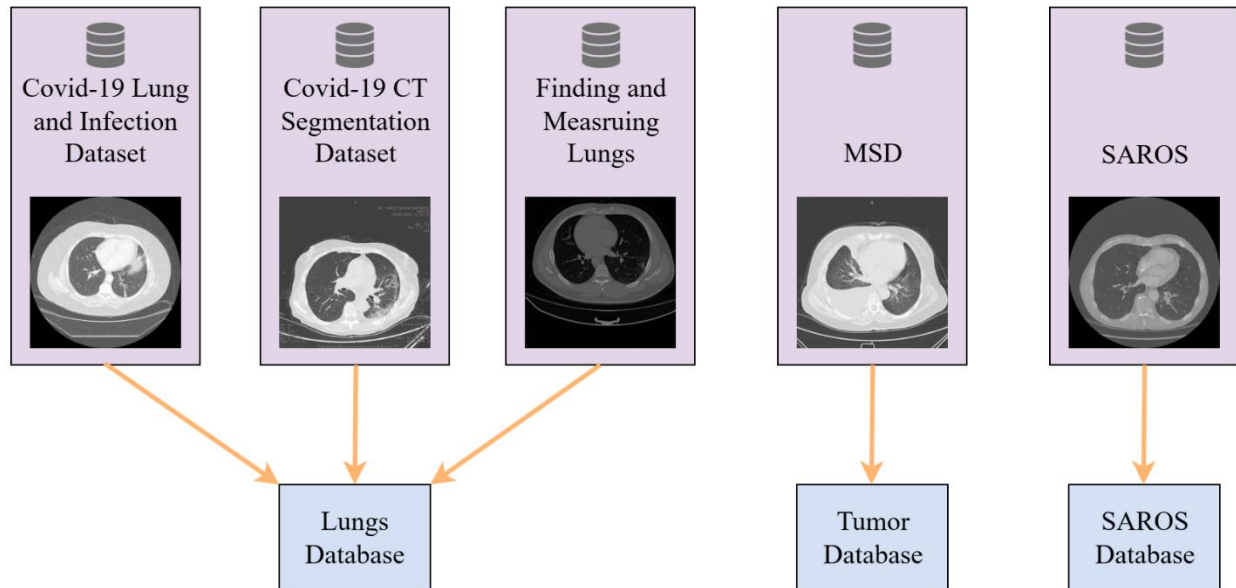

Figure 3.2 Representative CT slices from the datasets incorporated in this study. Lung database is compiled from three datasets, while the tumor and SAROS database contain one source each.

3.3 Data Augmentation & Split

To ensure the robustness of our study, each of the three databases is partitioned into identical 5-folds cross-validation splits. 80% of the data is used for training and 20% for testing. The validation sets contain an additional 20% from the training sets. Within the 5 folds of the lung database, the train, validation, and test splits comprise approximately 2953, 739, and 924 images respectively per fold. In order to expand the size, we utilize geometric augmentation approaches. The training set is augmented by incorporating horizontal flips and small translation operations, resulting in a total of 8859 images. Similarly, for the tumor database [31], the train, validation, test splits stand at 783, 196, 245 images respectively. Due to the relatively smaller number of data, a broader range of geometric augmentations is applied to this database, including horizontal and vertical flip, translation operations, and rotation; making the total count of images in the training set 3915 in each fold. Finally, the SAROS database [34], includes 3528, 882, and 1103 images in its training, validation and test splits per fold. Applying geometric augmentations such as are horizontal flips and translation operations with a probability of 0.20, increase the number of images in the training set to 5233 images.

3.4 Segmentation Models

In this section, we elaborate the architecture of our three deep learning networks – LungNet, MediNet, and TumorNet, designed and trained to generate segmentation masks for the lungs, mediastinum, and tumor. The networks follow a similar base model architecture, inspired by U-Net [36]. The U-Net architecture [36] is one of the most impactful architectures widely adopted for biomedical image segmentation. The U-shaped structure of U-Net divides the network into two primary paths: the encoder path for contraction and the decoder path for expansion. The encoder is composed of multiple convolutional layers followed by the activation function Rectified Linear Unit (ReLU) and max-pooling operations. As the input progresses through the encoder, the spatial dimensions of the feature maps decrease, while the number of channels increases, enabling the network to capture a hierarchical representation of the image. After the encoder, the bottleneck stage processes the image in a compressed form, allowing the network to interpret the global context of the image. The decoder path then works to restore the feature map's original spatial dimensions. U-Net's use of skip connections—linking feature maps from each encoder stage to the corresponding decoder stage—enables the integration of high-level structural information and detailed features, which improves segmentation accuracy. The U-Net architecture has been further enhanced by researchers using more complex encoder and decoder networks [37], [38], [39]. For example, ResNet [40] and DenseNet [41] are often chosen as encoders. ResNet is a transformatory architecture that introduces residual connection to train the deeper layers of the network more efficiently and minimize the problem of vanishing gradients. DenseNet, on the other hand, incorporates dense connections between layers, allowing each layer to acquire feature maps from all preceding levels. For the decoder part, the standard U-Net decoder structure is widely used due to its effectiveness in progressively restoring the resolution of feature maps. The decoder works by expanding the feature maps back to the input image's original spatial dimensions through up-convolutions, while incorporating skip connections from the encoder. This process ensures that the decoder is enriched with detailed features that help in reconstructing high-quality segmentation outputs. Another popular decoder is the Feature Pyramid Network (FPN) [42]. FPN utilizes a hierarchical framework comprising encoder and decoder components arranged in a pyramid-like structure, generating intermediate segmentation predictions at various spatial resolutions along the decoder pathway. Ultimately, these intermediate feature maps are resized to match spatial dimensions, combined, and processed through a convolutional layer with a 3 × 3 kernel. Finally, a SoftMax activation function is

applied to yield the segmentation mask. Further advancing the U-Net paradigm, UNet++ [43] has been proposed to address some limitations of the original U-Net, particularly in capturing finer-grained details and improving segmentation accuracy for objects of varying scales. Unlike the simple skip connections in U-Net, UNet++ redesigns these pathways to connect the encoder and decoder through a series of nested, dense convolutional blocks. The dense skip connections enable the aggregation of features from multiple scales within the decoder, leading to more precise delineation of object boundaries and better performance on complex segmentation tasks. The following sections describe each network in great details.

3.4.1 LungNet

For accurate T-stage classification, an important criterion is to assess whether the tumor is completely surrounded by lung tissues, or approaching the lung walls. A tumor that is fully encased within lung parenchyma and measures less than 3 cm in its largest axis is categorized as T1. Hence, LungNet is implemented for producing high-quality lung segmentation masks, which are to be used to evaluate this condition. Lung masks are also utilized to approximate the diaphragm position, as diaphragmatic invasion reclassifies the tumor stage as T4. The E-D CNN network in LungNet uses DenseNet-121 as its encoder. This works efficiently as each layer in the network is connected to all the other layers during the feed-forward phase. As a result, each layer accepts all its previous layers as inputs and enhances feature reusability. For the decoder stage, U-Net's decoder has shown great performance in the way it increases and restores the resolution of the encoder output as well as refines it by using skip connections in our proposed model, followed by the final 1x1 convolution. Hence, crucial spatial details and fine-grained features are maintained during boundary delineation in the lungs. This architecture demonstrates robust performance in generating reliable lung masks during inference on the primary dataset.

3.4.2 MediNet

The second segmentation module in the AnatomicalNets framework is MediNet, developed and trained for mediastinum segmentation. This is a significant step to classify T-stage as tumor invasion into the mediastinum will directly assign the stage to T-4, irrespective of the tumor size. For this model, we again utilize DenseNet121 as the encoder. But unlike in LungNet, the decoder component is based on the UNet++ architecture. This combination of a DenseNet121 encoder and a UNet++ decoder allows our model to leverage the strengths of both architectures: the feature representation power of DenseNet and the improved feature aggregation of UNet++. The effectiveness of this design is further validated by its strong performance on both annotated and primary datasets.

3.4.3 TumorNet

Finally, tumor segmentation masks are acquired through the implementation of TumorNet. The encoder backbone consists of a ResNet-152 model, chosen for its depth and ability to extract detailed hierarchical features. The decoder utilizes a Feature Pyramid Network (FPN), designed to effectively reconstruct segmentation masks by combining multi-scale feature maps generated by the ResNet-152 encoder. TumorNet operates on cropped tumor ROI from CT images, enabling focused segmentation of tumor structures. Deploying task specific encoder-decoder architecture enables us to achieve the highest level of performance which is evident in the results section of our experiments.

3.5 Lung Tumor Detection

As illustrated in figure 3.1, a dedicated lung tumor detection model, based on the YOLOv11 architecture is trained on the primary Lung-PET-CT-Dx dataset. This model detects tumor regions in CT images using a bounding box. These serve as inputs to TumorNet during segmentation inference. The

detection model is an integral part of our pipeline. While training TumorNet, the tumor region in the annotated tumor database is cropped and padded to generate the tumor's segmentation mask. However, since there is no ground truth tumor segmentation mask in the primary dataset, we deploy a detection model to generate tumor ROIs for each CT slice. The detected bounding boxes are used for mask generation in our cross-dataset inference strategy. For the detection model, YOLOv11 architecture has been implemented. The architecture of YOLOv11 represents a significant enhancement over previous versions. YOLOv11 incorporates new layers, blocks, and optimizations that enhance both computational efficiency and detection accuracy. The convolutional layers assist in gradually decreasing the spatial resolution, as it increases the feature map depth. Another special aspect of YOLOv11 is that it uses C3k2 block instead of C2f block. It is a more efficient block based on the Cross-Stage-Patrial (CSP) network. Our lung tumor detection model shows high mean Average Precision (mAP) scores, providing accurate bounding boxes across CT slices.

3.6 Mask Inference

 T-stage classification depends heavily on the tumor's size and distance properties. The primary dataset [23] does not include ground truth masks for any of the desired anatomical structures. The modules within the AnatomicalNets are therefore trained to be applied to the primary dataset. The LungNet, MediNet, and TumorNet generates ground truth segmentation masks for the lung, mediastinum, and tumor respectively by treating Lung-PET-CT-Dx as an external validation set. The inferred masks serve as surrogate ground truth data, enabling further analysis and research on the dataset, where manual annotations are otherwise unavailable. A randomly selected subset of the generated masks are reviewed and approved by three expert clinicians for qualitative assurance. In figure 3.3, sample CT images and inferred ground truth masks are shown, demonstrating the precision of the generated lung, mediastinum, and tumor masks.
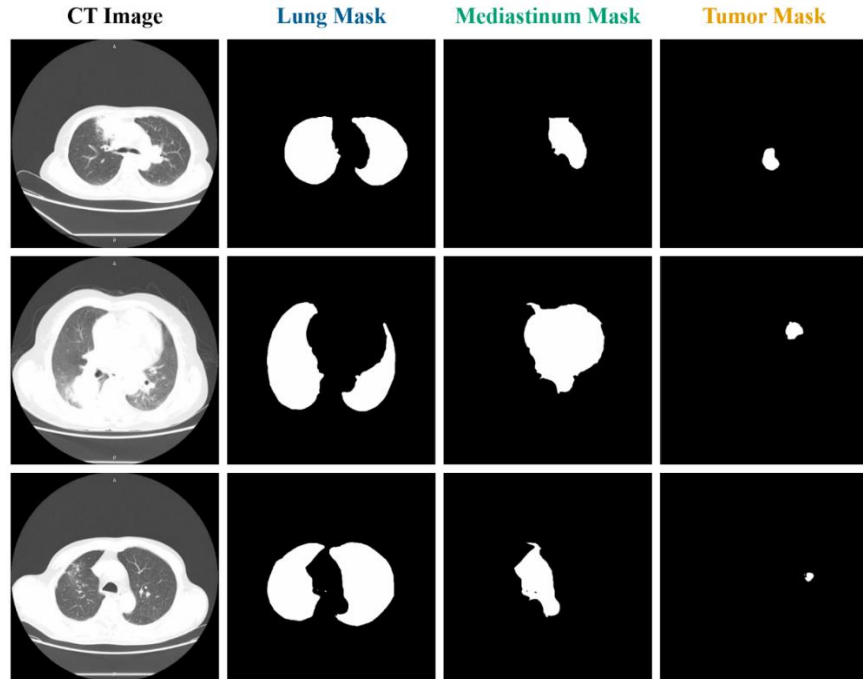
Figure 3.3 CT images (first column) alongside corresponding lung masks (second column), mediastinum masks (third column), and tumor masks (fourth column) generated through cross-dataset inference.

3.7 Diaphragm Estimation

As discussed earlier, extracting diaphragmatic invasion is critical for T-stage classification. However, publicly available datasets specifically annotated for diaphragm segmentation are limited or unavailable. To overcome this challenge, we develop a specialized estimation technique leveraging the inferred lung segmentation masks of the Lung-PET-CT-Dx dataset. Our method involves a pixel-based approach along the lung mask contours. Specifically, the two lowest pixels at the inferior boundary of the lung masks are first identified. From these points, an upward region extending approximately 10% of the lung mask's height is extracted. The choice of 10% is not random but rather obtained from a rigorous trial and error process, indicating that this method provides the best results. Additionally, insights from studies regarding the estimation of the diaphragm's position [44] has aided in making this strategy. This strategy enables reliable estimation of the diaphragm's position without requiring additional segmentation models, offering a practical and efficient alternative. Figure 3.4 illustrates the step-by-step procedure for estimating the diaphragm position.
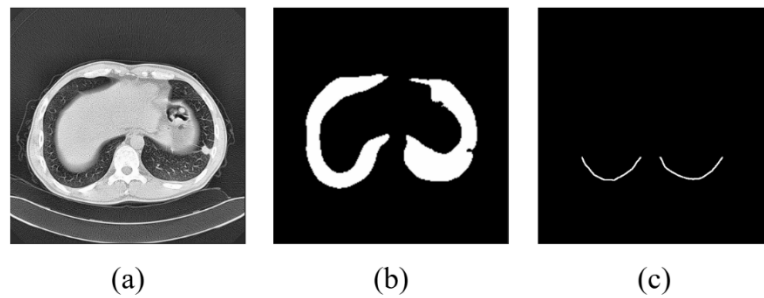

(a)   (b)   (c)

Figure 3.4 (a) A sample CT image from the primary Lung-PET-CT-Dx dataset. (b) The corresponding lung segmentation mask generated from the CT image. (c) The estimated diaphragm position derived from the lung segmentation mask, used for further anatomical analysis.

3.8 Quantitative Measurement of Tumor Properties

The second phase of the proposed pipeline involves computing the tumor properties essential for classifying T-stage. In clinical practice, to determine the T-stage, experts evaluate both the size and location of the tumor - particularly in relation to potential invasion of adjacent structures. To reflect this clinical context, we calculate the following quantitative metrics from each patient's CT scan:

- Maximum tumor dimension.
- Distance between the tumor and the lung walls.
- Distance between the tumor and the estimated diaphragm.
- Distance between the tumor and the mediastinum.

These distances are measured by first extracting the contours of the generated ground truth segmentation masks. Next, we compute the maximum distance between the tumor contour and the corresponding anatomical region in pixels. Finally, the pixel distance is multiplied with the pixel spacing of the CT slices to get the distance in practical units. This process ensures that the greatest spatial separation between the

tumor and its neighboring structures is captured, which is crucial for determining the existence of any invasion. A distance of zero is interpreted as direct invasion of the corresponding structure. In addition to this, the tumor's largest dimension is determined. Considering that it can be either in the width, heigh, or depth dimension, two different approaches have been adopted. First, the contour outline of the tumor segmentation mask is analyzed to measure the largest euclidean distance between contour points, multiplied by the pixel spacing of the CT slice. Additionally, to estimate the tumor's depth, the number of slices containing visible tumor regions is multiplied by the slice thickness of the CT scan. Finally, the two dimensions are compared and the larger measurement is assigned as the tumor size. These extracted properties contribute to the overall assessment of the tumor's volume and extent. Figure 3.5 illustrates a rough visualization of the contours.
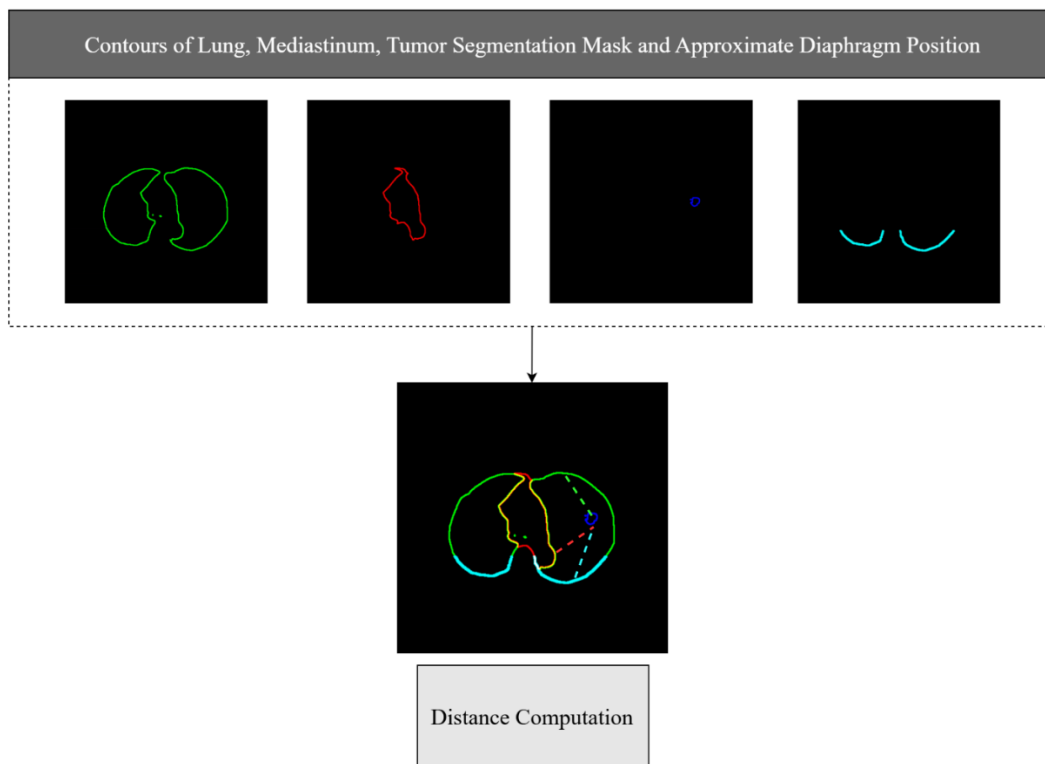

Figure 3.5 Visualization of the approach used to measure the key distances. The first row illustrates the contours obtained from the generated masks. In the single image in the second row, the contour images are superimposed and the maximum distances between the tumor and key anatomical structures are indicated using a dashed line ('red' for mediastinum, 'blue' for diaphragm, 'green' for lungs).

3.9 T-Stage Classification

The final phase of our proposed workflow is the classification of lung cancer T-stage among patients. In this step, we utilize the extracted tumor properties to perform a condition-based T-staging. Following the previous phases, we have the tumor size, the knowledge of any invasion of tumor into the lung walls, mediastinum, or the diaphragm. Now we constrain them into conditions set by the IASLC guidelines. The conditions and the decision-making process is detailed in the flowchart 3.6. All these

conditions are in accordance with the IASLC guidelines. By adhering to the medical guidelines, our method is not only highly accurate, but also medically reliable and reproducible.
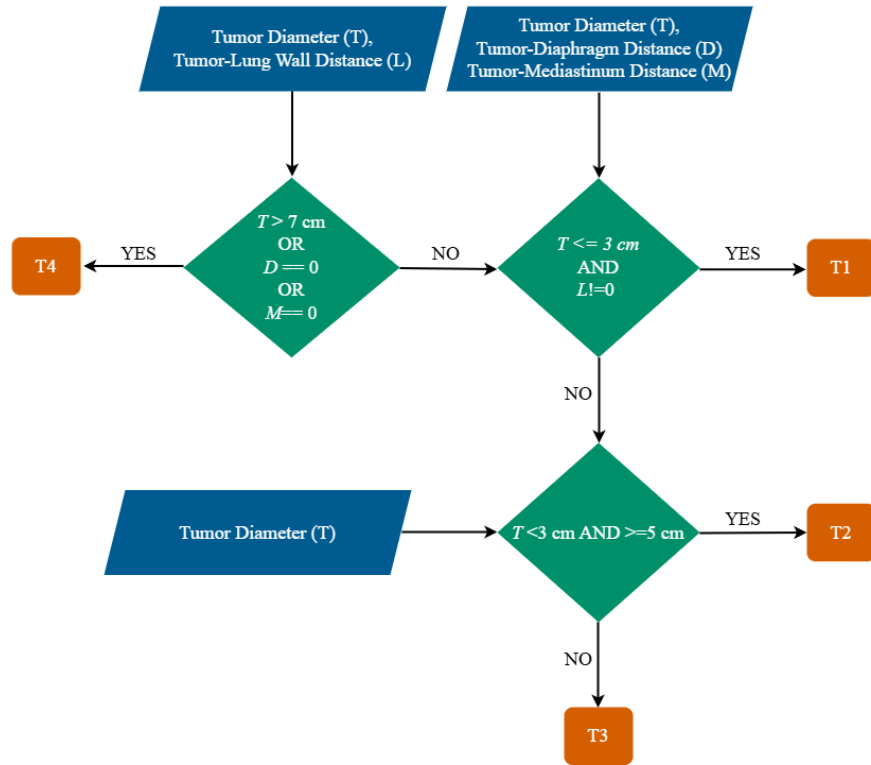

Figure 3.6 A flowchart describing the step-by-step decision-making process for T-stage classification on the basis of tumor size and invasion into other anatomical structures.

4. Experiment

This section outlines the experimental framework utilized in our study. We talk about the experimental setup of the architectures in AnatomicalNets, as well as the detection model using YOLOv11.

4.1 Experimental Setup

To achieve the best performance in all of the networks, task specific training parameters are used. The training parameters look similar for all the architectures except for the loss function, which has been adapted depending on the network's purpose. Experiments are conducted on a local workstation equipped with an Intel® Core™ i9-14900KF CPU at 3.20 GHz and 32 GB of RAM, running a 64-bit x64 architecture. The software environment comprises Python 3.10.6 and PyTorch 2.6.0+cu118. A number of state-of-the-art deep learning models are implemented using the Segmentation Models PyTorch (SMP) package (Iakubovskii). For AnatomicalNets, all advanced encoders used are initialized with pretrained weights trained on the ImageNet dataset [45]. The optimization of the loss function is performed using the Adam method, with a constant learning rate (α = 0.00001) in the segmentation networks. In the detection model, Stochastic Gradient Descent (SGD) has been used as the optimizer. During the training phase, an early stopping criterion is employed: if no significant improvement in validation loss was observed for 20 consecutive epochs, training was immediately terminated. Hyperparameter and training parameter details are provided in Table 2 and 3.

Table 2 Segmentation network training parameters

Training Parameters	Parameter Value (LungNet)	Parameter Value (MediNet)	Parameter Value (TumorNet)
Batch size	64	64	64
Learning Rate	1e-4	1e-4	1e-4
Number of folds	5	5	5
Max epochs	100	100	100
Epoch Patience	5	5	5
Epoch Stopping Criteria	20	20	20
Encoder Weight	ImageNet	ImageNet	ImageNet
Optimizer	Adam	Adam	Adam
Loss Function	DiceLoss	DiceLoss	0.5*DiceLoss + 0.5*JaccardLoss
Encoder Depth	5	5	5

Table 3 Tumor Detection Network (YOLOv11) training parameters

Training Parameters	Parameter Value
Batch size	16
Image Size	640x640
Momentum	0.9
Mosaic	True
Label Smoothing	0
Max epoch	100
Optimizer	SGD

4.2 Loss Function

Our framework describes three modules for the segmentation of the lung, mediastinum, and lung tumor in the CT slices. In LungNet and MediNet, to segment the lung and mediastinum, DiceLoss has been

used. For TumorNet, we optimize our model with a richly descriptive, overlap-based loss that combines two complementary measures of mask similarity—Dice and Jaccard—in order to both counteract class imbalance and sharpen boundary delineation. The Dice component derives from the Dice Similarity Coefficient (DSC) originally formulated to quantify volumetric overlap in medical imaging; it naturally ranges between 0 (no overlap) and 1 (perfect agreement), making it particularly effective when the region of interest occupies only a small fraction of the scan and models tend to over-predict the background. Since the classical DSC is non-differentiable, we employ the probabilistic variant, defined for a binary mask as:

$$L_{Dice} = 1 - \frac{\left(2 \sum_{\{j=1\}}^{N} y_j p_j + \epsilon\right)}{\left(\sum_{\{j=1\}}^{N} y_j + \sum_{\{j=1\}}^{N} p_j + \epsilon\right)} \tag{1}$$

where $pj \in [0,1]$ is the model's predicted probability at pixel jj, $yj \in \{0,1\}$ is the corresponding ground-truth label, N is the total number of pixels, and ϵ is a small smoothing constant to guard against division by zero. To further penalize false positives at object boundaries and reinforce overall region overlap, we augment this with the Jaccard (IoU) loss:

$$L_{\{Jaccard\}} = 1 - \frac{\left(\sum_{\{j=1\}}^{N} y_j p_j + \epsilon\right)}{\left(\sum_{\{j=1\}}^{N} y_j + \sum_{\{j=1\}}^{N} p_j - \sum_{\{j=1\}}^{N} y_j p_j + \epsilon\right)} \tag{2}$$

By weighting both terms equally, our final overlap loss becomes

$$L_{\{overlap\}} = 0.5 L_{\{Dice\}} + 0.5 L_{\{Jaccard\}} \tag{3}$$

This balanced formulation ensures that the network receives strong gradient signals both where regions should coincide (via the Dice term) and where their intersection over union must be maximized (via the Jaccard term), leading to robust and precise tumor segmentation in challenging, low-contrast medical imagery.

4.3 Evaluation Metrics

In this section, the evaluation metrics used in each step of the workflow are described. In evaluating segmentation performance, this research utilizes a comprehensive array of measures. In addition to familiar indicators such as precision, Intersection over Union (IoU), recall (sensitivity), we also apply the Dice Similarity Coefficient (DSC), overall accuracy, False Negative Rate (FNR), False Positive Rate (FPR), and specificity. Among these, IoU and DSC serve as the primary metrics for this portion of the analysis. The metrics can be defined as follows:

$$IoU = \frac{TP}{TP + FP + FN} \tag{4}$$

$$DSC = \frac{2TP}{2TP + FP + FN} \tag{5}$$

$$Accuracy = \frac{TP + TN}{TP + TN + FP + FN} \tag{6}$$

$$Precision = \frac{TP}{TP + FP} \tag{7}$$

$$Sensitivity = \frac{TP}{TP + FN} \tag{8}$$

$$Specificity = \frac{TN}{TN + FP} \tag{9}$$

$$FNR = \frac{TP * FN}{TP + FN} \tag{10}$$

$$FPR = \frac{FP}{FP + TN} \tag{11}$$

Here, TP, FP, FN refers to true positive, false positive, and false negative respectively. IoU and DSC are the most impactful metrics to evaluate the consistency between ground truth mask and predicted mask. There is a slight difference in the way these two metrics are calculated. IoU evaluates the overlap by determining the ratio of the intersection to the union of the predicted and ground truth seg mentation masks. Conversely, DSC measures overlap by considering the proportion of the intersection relative to the total aggregate area of the predicted and ground truth segmentations.

To rigorously assess the performance of our tumor detection module, several quantitative evaluation metrics were employed, computed individually across each fold and averaged across all five folds for robust analysis. The metrics utilized include Precision, Recall, F1 Score, mean Average Precision (mAP) at IoU thresholds of 0.5 (mAP50) and between 0.5 to 0.95 (mAp50-95).

The F1 Score represents the harmonic mean of precision and recall, providing a balanced measure between false positives and false negatives:

$$F1\ Score = \frac{2 * Precision * Recall}{Precision + Recall} \tag{12}$$

Additionally, the mAP was computed at two standard thresholds. The mAP50 is defined as the mean Average Precision at an IoU threshold of 0.5, serving as a commonly used benchmark in detection tasks. The \ mAP50-95 metric averages the precision across a range of IoU thresholds from 0.5 to 0.95, penalizing localization inaccuracies and providing a comprehensive performance perspective:

$$mAP = \frac{1}{N} \sum_{i=1}^{N} AP_i \tag{13}$$

5 Results and Discussion

This section presents an extensive analysis of the performance of the segmentation and detection experiments conducted in the study, as well as the size and invasion-based T-stage classification, offering a detailed report of the results. We also compare our results with results obtained from implementing most common CNN architectures for the classification of T-stage.

5.1 Results of the AnatomicalNets

Table 4 presents an extensive analysis of performance metrics regarding LungNet, MediNet, and TumorNet. This incorporates a comparison among five different deep learning networks— UNet, DenseNet121-UNet, DenseNet121-UNet++, ResNet50-UNet, and Resnet152-FPN. The assessment criteria comprise Accuracy (AC), Dice Score (DSC), Intersection over Union (IoU), Precision (P), Sensitivity (SN), Specificity (SP) , FNR, and FPR. This comparative analysis aims to determine which deep learning network and preprocessing technique is the most effective in segmenting the lungs from CT images. Applying the same five encoder-decoder structures keeps the consistency among different models and also provides information on which design is most suitable for the intended task.

5.2 Results of Tumor Detection Module

Table 5 presents an extensive analysis of performance metrics regarding the tumor detection model. Thos is trained to predict the tumor ROI in the Lung PET-CT-Dx dataset. YOLOv11 has shown the best detection results in terms of the most important metric mAP50-95 and other metrics. YOLOv10 and YOLOv8 have also been utilized to show the difference in performance and to further emphasize the impact of using YOLOv11. The evaluating metrics highlighted in this analysis are: Precision (P), Recall (R), mAP50, and mAP50-95. This analysis indicates to the efficacy of the YOLOv11 detection model to localize the tumor region from CT images. Similar to the segmentation models, these are averaged results from the described five folds.

5.3 Results of T-stage Classification

The core objective of this study is accurate classification of the T-stage of lung cancer patients. To keep this classification process aligned with the clinically acclaimed guidelines, we opt for a method that does this classification based on tumor size and its invasion into other significant structures. This novel approach achieves high metrics among all significant metrics. The metrics evaluated in the classification task are Accuracy (Acc), Precision (P), Recall (R), and F1 Score. The classification is done according to the procedure described in Section 3.9. The classification report is summarized in Table 6 and a confusion matrix is provided in Figure 5.1. The proposed methodology achieves an overall accuracy of 91.36%. The detailed breakdown of precision, recall, and F1 score for each T stage (T1,T2,T3,T4) further highlights the efficacy of the methodology. All classes achieve high F1 score indicating the robustness of the model in classifying the stages. The confusion matrix illustrates a pattern in the cases the approach failed to make the correct predictions. To further validate the proposed methodology over traditional image classification networks, a comparison in performance is demonstrated in Table 7 between our approach and most widely adopted CNN architectures. These differences indicate to the credibility and necessity of the adopted approach even more.

Table 4 Model performance comparison for the three anatomical segmentation models.

Model Name	Network	Acc (%)	IoU (%)	DSC (%)	P (%)	SN (%)	SP (%)	FNR (%)	FPR (%)
LungNet	UNet	97.26	91.59	93.56	94.00	93.76	98.30	6.24	1.70
	DenseNet 121-UNet++	97.60	92	94.28	84.04	95.64	98.59	4.36	1.41
	Densenet 121 - Unet	**98.96**	**96.07**	**97.82**	**97.27**	**96.85**	**99.37**	**3.15**	**0.63**
	ResNet50-UNet	97.19	92.87	95.02	94.58	94.0	98.50	6.0	1.50
	ResNet152-FPN	97.88	92.79	95.98	95.64	94.56	98.79	5.44	1.21
MediNet	UNet	97.62	88.76	91.89	90.58	89.64	94.09	10.36	5.91
	DenseNet 121-UNet++	**98.06**	**90.46**	**93.39**	**91.78**	**92.80**	**96.63**	**7.2**	**3.37**
	Densenet 121 - Unet	97.71	89.13	92.17	90.92	91.98	96.21	8.02	3.79
	ResNet50-UNet	96.78	85.92	88.47	88.21	88.76	95.03	11.24	4.97
	ResNet152-FPN	97.01	86.58	89.14	88.95	89.39	95.41	10.61	4.59
TumorNet	UNet	97.76	80.10	85.74	87.82	84.56	98.55	15.44	1.45
	DenseNet 121-UNet++	97.90	81.22	86.63	88.04	84.26	99.51	15.74	0.49
	Densenet 121- Unet	97.88	81.76	86.45	88.39	84.85	99.53	15.15	0.47
	ResNet50-UNet	97.66	79.09	85.25	85.33	87.33	99.52	12.67	0.48
	ResNet152-FPN	**97.93**	**83.43**	**89.68**	**89.40**	**88.15**	**99.55**	11.85	**0.45**

Table 5 Model performance comparison for the tumor detection model.

Network	P (%)	R (%)	mAP50 (%)	mAP50-95 (%)
YOLOv8	85.80	83.87	86.0	45.37
YOLOv10	91.0	91.0	92.3	58.6
YOLOv11	**93.0**	**92.3**	**94.3**	**60.0**

Table 6 Classification results of lung cancer T-stage

T stages	Acc (%)	P (%)	R (%)	F1 Score
T1	91.36	96.0	90.0	93.0
T2		90.0	88.3	89.9
T3		97.0	96.0	96.0
T4		88.0	90.0	90.0

Table 7 Comparison of Performance with Traditional CNN Approach.

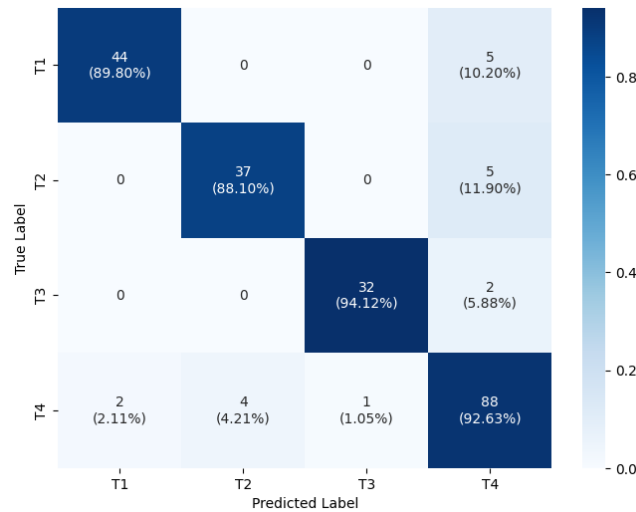| Network	Acc (%)	P (%)	R (%)	F1Score (%)
ResNet152	37.29	39.04	37.29	36.71
DenseNet121	40.35	39.80	39.8	39.81
SwinTransformer	39.28	40.08	39.28	39.04
Proposed Model	**91.36**	**96.0**	**90.0**	**92**

Figure 5.1 Confusion Matrix illustrating the performance of the proposed novel T stage classification approach

Table 6 portrays the robustness and reliability of the proposed framework, highlighting consistently high F1 scores ranging from 89% to 96% across different tumor stage categories. This indicates the model's strong capability in accurately distinguishing each class Table 7 provides a comprehensive comparative analysis with existing CNN-based approaches. These methods exhibit a maximum average F1 score of

39.81% and an accuracy is 40.35%, significantly inferior to our results. These findings support the approach of adopting a clinically informed framework to tumor staging.

5.4 A Deeper Look into the Wrong Predictions

It is observable from Table 6 and Figure 6.1 that stage T4 has the lowest precision and the second lowest F1 score among all the stages. This can be explained using clinical rationale. Key points to consider include:

- **Multifocal Disease as a T4 Criterion:** A key criterion for T4 classification in lung cancer is the presence of separate tumor nodules in a different ipsilateral lobe than the primary tumor [46], [47] . A patient with such tumor nodules is classified as T4, regardless of the individual nodule sizes or the extent of invasion of contiguous structures by any single nodule. In our proposed pipeline, which primarily assesses individual nodule characteristics (size) and their distances to anatomical landmarks, a patient with, for instance, a 2 cm nodule in the upper lobe and a 1.5 cm nodule in the lower lobe could be erroneously classified as T1 or T2 based solely on these individual measurements. This limitation significantly contributes to the observed misclassification of true T4 cases as earlier stages.

- **Limited Scope of Invaded Structures in T4 Definition:** The misclassification of T4 is also significantly influenced by the limited range of invaded structures considered by our model. According to the AJCC 8th Edition TNM classification, a primary lung tumor is classified as T4 if it directly invades any of the following structures: diaphragm, mediastinum, heart, great vessels (e.g., aorta, superior vena cava, pulmonary artery/veins), trachea, recurrent laryngeal nerve, esophagus, vertebral body, or carina [46], [47], [48]. Our model's features are restricted to distance measurements from only the diaphragm, mediastinum, and the lung walls. While our method presents a novel approach and is among the first works to address staging in a clinically relevant manner using such features, this narrow focus represents a significant limitation causing these misclassifications.

These points collectively highlight the inherent complexity of diagnosing the T4 stage and directly indicate the limitations of this study's current feature set. Figure 6.2 illustrates a few examples of these misclassified T4 cases.

Table 8 Examples of Misclassified CT Images in T4 Stage

CT Image	Predicted Stage	Ground Truth	Rationale for Misclassification
	T2	T4	Misclassification possibly due to the presence of

	T3	T4	secondary tumor nodules or invasion into anatomical structures not considered by the model
	T1	T4	

5.5 Limitations & Future Work

In this study, we have demonstrated a novel hybrid framework that integrates deep-learning–based segmentation of key thoracic structures with intuitive, rule-based measurements, yielding interpretable T-stage classifications at a high accuracy. However, there are some limitations of this approach. Addressing the limitations could be the used as a motivation for the future work in this domain of research. Our diaphragm boundary relies on a simple heuristic using the lowest 10 % of lung mask points, due to the lack of datasets related to diaphragm segmentation. It may misalign in atypical anatomies. Also, our evaluation remains confined to a single 2D CT dataset. By focusing solely on two-dimensional slices, we may overlook volumetric tumor characteristics that could refine staging. Again, according to the IASLC guidelines, the staging of lung tumor also depends on some more regions visible in the CT scan such as the trachea, esophagus, carina etc. In future work, we plan to curate or annotate a true diaphragm segmentation set to replace our heuristic, extend the pipeline to full 3D segmentation for more accurate tumor depth assessment, and perform segmentation of more regions in order to broaden validation across multi-center cohorts. Finally, we aim to expand our approach to complete TNM staging by integrating lymph node and metastasis detection models to further enhance clinical applicability.

6 Conclusion

This study proposed a novel, transparent, clinically informed framework for lung cancer T-stage classification that synergizes deep learning–based segmentation with rule-based measurement protocols. By explicitly modeling anatomical context and adhering to IASLC criteria, our method attains 91.36% accuracy and robust per-stage performance across four tumor stages. The approach bridges the gap between "black-box" classifiers and clinical practice, offering interpretable outputs that can readily integrate into radiological workflows. Future enhancements—such as refined diaphragm segmentation, 3D modeling, and expansion to full TNM staging—will further elevate its utility and generalizability in real-world settings.

Declaration of generative AI and AI-assisted technologies in the manuscript preparation process

During the preparation of this work the authors used ChatGPT 4 in order to refine language, check grammar and punctuation, and enhance the overall readability and conciseness. After using this tool, the authors

reviewed and edited the content as needed and take full responsibility for the content of the published article.

References

[1]   S. J. Olshansky, B. A. Carnes, and D. Grahn, "Confronting the Boundaries of Human Longevity: Many people now live beyond their natural lifespans through the intervention of medical technology and improved lifestyles—a form of" manufactured time"," *American Scientist,* vol. 86, no. 1, pp. 52-61, 1998.

[2]   A. Leiter, R. R. Veluswamy, and J. P. Wisnivesky, "The global burden of lung cancer: current status and future trends," *Nature reviews Clinical oncology,* vol. 20, no. 9, pp. 624-639, 2023.

[3]   W. Sun, B. Zheng, and W. Qian, "Computer aided lung cancer diagnosis with deep learning algorithms," in *Medical imaging 2016: computer-aided diagnosis*, 2016, vol. 9785: SPIE, pp. 241-248.

[4]   S. Lakshmanaprabu, S. N. Mohanty, K. Shankar, N. Arunkumar, and G. Ramirez, "Optimal deep learning model for classification of lung cancer on CT images," *Future Generation Computer Systems,* vol. 92, pp. 374-382, 2019.

[5]   L. Wang, "Deep learning techniques to diagnose lung cancer," *Cancers,* vol. 14, no. 22, p. 5569, 2022.

[6]   T. L. Chaunzwa *et al.*, "Deep learning classification of lung cancer histology using CT images," *Scientific reports,* vol. 11, no. 1, pp. 1-12, 2021.

[7]   J. A. Barta, C. A. Powell, and J. P. Wisnivesky, "Global epidemiology of lung cancer," *Annals of global health,* vol. 85, no. 1, p. 8, 2019.

[8]   J. Zhou, Y. Xu, J. Liu, L. Feng, J. Yu, and D. Chen, "Global burden of lung cancer in 2022 and projections to 2050: Incidence and mortality estimates from GLOBOCAN," *Cancer Epidemiology,* vol. 93, p. 102693, 2024.

[9]   V. Ambrosini *et al.*, "PET/CT imaging in different types of lung cancer: an overview," *European journal of radiology,* vol. 81, no. 5, pp. 988-1001, 2012.

[10]   W. J. Petty and L. Paz-Ares, "Emerging strategies for the treatment of small cell lung cancer: a review," *JAMA oncology,* vol. 9, no. 3, pp. 419-429, 2023.

[11]   R. U. Osarogiagbon *et al.*, "The International Association for the Study of Lung Cancer Lung Cancer Staging Project: overview of challenges and opportunities in revising the nodal classification of lung cancer," *Journal of Thoracic Oncology,* vol. 18, no. 4, pp. 410-418, 2023.

[12]   K. H. Weerakkody Y, Worsley C. "Lung cancer (staging - IASLC 8th edition)." https://radiopaedia.org/articles/lung-cancer-staging-iaslc-8th-edition (accessed.

[13]   Y. Zhong *et al.*, "Deep learning for prediction of N2 metastasis and survival for clinical stage I non–small cell lung cancer," *Radiology,* vol. 302, no. 1, pp. 200-211, 2022.

[14]   Ö. Önal, M. Kocer, H. N. Eroğlu, S. D. Yilmaz, I. Eroğlu, and D. Karadoğan, "Survival analysis and factors affecting survival in patients who presented to the medicaloncology unit with non-small cell lung cancer," *Turkish Journal of Medical Sciences,* vol. 50, no. 8, pp. 1838-1850, 2020.

[15]   I. M. Israel, S. A. Israel, and J. M. Irvine, "Factors influencing CNN performance," in *2021 IEEE Applied Imagery Pattern Recognition Workshop (AIPR)*, 2021: IEEE, pp. 1-4.

[16]   H.-C. Chu, H.-C. Lai, M.-Y. Wang, and S.-J. Wu, "CNN Distance Estimation Based on Received Signal Strength Indicator," in *2024 IEEE International Conference on Systems, Man, and Cybernetics (SMC)*, 2024: IEEE, pp. 2103-2107.

[17]   M. A. Heuvelmans *et al.*, "Lung cancer prediction by Deep Learning to identify benign lung nodules," *Lung cancer,* vol. 154, pp. 1-4, 2021.

[18]   W. Hendrix *et al.*, "Deep learning for the detection of benign and malignant pulmonary nodules in non-screening chest CT scans," *Communications medicine,* vol. 3, no. 1, p. 156, 2023.

[19]   T. Adams, J. Dörpinghaus, M. Jacobs, and V. Steinhage, "Automated lung tumor detection and diagnosis in CT Scans using texture feature analysis and SVM," in *FedCSIS (Communication Papers)*, 2018, pp. 13-20.

[20]   M. A. Khan *et al.*, "VGG19 network assisted joint segmentation and classification of lung nodules in CT images," *Diagnostics,* vol. 11, no. 12, p. 2208, 2021.

[21]   K. Barbouchi, D. El Hamdi, I. Elouedi, T. B. Aïcha, A. K. Echi, and I. Slim, "A transformer-based deep neural network for detection and classification of lung cancer via PET/CT images," *International Journal of Imaging Systems and Technology,* vol. 33, no. 4, pp. 1383-1395, 2023.

[22]   K. Simonyan and A. Zisserman, "Very deep convolutional networks for large-scale image recognition," *arXiv preprint arXiv:1409.1556,* 2014.

[23]   P. Li, Wang, S., Li, T., Lu, J., HuangFu, Y., & Wang, D. . *A Large-Scale CT and PET/CT Dataset for Lung Cancer Diagnosis (Lung-PET-CT-Dx) [Data set]*, doi: https://www.cancerimagingarchive.net/collection/lung-pet-ct-dx/#citations.

[24]   S. G. Armato III, McLennan, G., Bidaut et al. *LIDC-IDRI | Data from The Lung Image Database Consortium (LIDC) and Image Database Resource Initiative (IDRI): A completed reference database of lung nodules on CT scans*, doi: https://www.cancerimagingarchive.net/collection/lidc-idri/#citations.

[25]   A. Wehbe, S. Dellepiane, and I. Minetti, "Enhanced Lung Cancer Detection and TNM Staging Using YOLOv8 and TNMClassifier: An Integrated Deep Learning Approach for CT Imaging," *IEEE Access,* 2024.

[26]   D. Reis, J. Kupec, J. Hong, and A. Daoudi, "Real-time flying object detection with YOLOv8," *arXiv preprint arXiv:2305.09972,* 2023.

[27]   X. Dai, Y. Chen, J. Yang, P. Zhang, L. Yuan, and L. Zhang, "Dynamic detr: End-to-end object detection with dynamic attention," in *Proceedings of the IEEE/CVF international conference on computer vision*, 2021, pp. 2988-2997.

[28]   B. K. Sathiyamurthy and V. K. Madhaiyan, "Automated lung cancer T-Stage detection and classification using improved U-Net model," *International Journal of Electrical & Computer Engineering (2088-8708),* vol. 14, no. 6, 2024.

[29]   R. Fan *et al.*, "T-stage diagnosis of lung cancer based on deep learning in CT images," *Digital Medicine,* vol. 10, no. 4, p. e00017, 2024.

[30]   J. Zhang and H. Zhang, "A Bayesian neural network model based on CT images for staging non-small cell lung cancer," in *2023 8th International Conference on Computer and Communication Systems (ICCCS)*, 2023: IEEE, pp. 884-893.

[31]   *Medical Segmentation Decathlon (MSD)*, doi: https://doi.org/10.1109/ISBI.2019.00030.

[32]   *COVID-19 CT segmentation dataset*. [Online]. Available: https://medicalsegmentation.com/covid19/

[33]   M. Jun *et al.*, "COVID-19 CT lung and infection segmentation dataset," *(No Title),* 2020.

[34]   S. Koitka *et al.*, "SAROS: A dataset for whole-body region and organ segmentation in CT imaging," *Scientific Data,* vol. 11, no. 1, p. 483, 2024.

[35]   K. S. Mader. *Finding and Measuring Lungs in CT Data*

[Online]. Available: https://www.kaggle.com/datasets/kmader/finding-lungs-in-ct-data

[36]   O. Ronneberger, P. Fischer, and T. Brox, "U-net: Convolutional networks for biomedical image segmentation," in *Medical image computing and computer-assisted intervention–MICCAI 2015: 18th international conference, Munich, Germany, October 5-9, 2015, proceedings, part III 18*, 2015: Springer, pp. 234-241.

[37]   R. Sarmun *et al.*, "Enhancing intima-media complex segmentation with a multi-stage feature fusion-based novel deep learning framework," *Engineering Applications of Artificial Intelligence,* vol. 133, p. 108050, 2024.

[38]   S. Kolhar and J. Jagtap, "Convolutional neural network based encoder-decoder architectures for semantic segmentation of plants," *Ecological Informatics,* vol. 64, p. 101373, 2021.

[39]   T. Lei, R. Wang, Y. Zhang, Y. Wan, C. Liu, and A. K. Nandi, "DefED-Net: Deformable encoder-decoder network for liver and liver tumor segmentation," *IEEE Transactions on Radiation and Plasma Medical Sciences,* vol. 6, no. 1, pp. 68-78, 2021.

[40]   K. He, X. Zhang, S. Ren, and J. Sun, "Deep residual learning for image recognition," in *Proceedings of the IEEE conference on computer vision and pattern recognition*, 2016, pp. 770-778.

[41]   G. Huang, Z. Liu, L. Van Der Maaten, and K. Q. Weinberger, "Densely connected convolutional networks," in *Proceedings of the IEEE conference on computer vision and pattern recognition*, 2017, pp. 4700-4708.

[42]   T.-Y. Lin, P. Dollár, R. Girshick, K. He, B. Hariharan, and S. Belongie, "Feature pyramid networks for object detection," in *Proceedings of the IEEE conference on computer vision and pattern recognition*, 2017, pp. 2117-2125.

[43]   Z. Zhou, M. M. Rahman Siddiquee, N. Tajbakhsh, and J. Liang, "Unet++: A nested u-net architecture for medical image segmentation," in *Deep learning in medical image analysis and multimodal learning for clinical decision support: 4th international workshop, DLMIA 2018, and 8th international workshop, ML-CDS 2018, held in conjunction with MICCAI 2018, Granada, Spain, September 20, 2018, proceedings 4*, 2018: Springer, pp. 3-11.

[44]   T. Suwatanapongched, D. S. Gierada, R. M. Slone, T. K. Pilgram, and P. G. Tuteur, "Variation in diaphragm position and shape in adults with normal pulmonary function," *Chest,* vol. 123, no. 6, pp. 2019-2027, 2003.

[45]   J. Deng, W. Dong, R. Socher, L.-J. Li, K. Li, and L. Fei-Fei, "Imagenet: A large-scale hierarchical image database," in *2009 IEEE conference on computer vision and pattern recognition*, 2009: Ieee, pp. 248-255.

[46]   P. Goldstraw *et al.*, "The IASLC lung cancer staging project: proposals for revision of the TNM stage groupings in the forthcoming (eighth) edition of the TNM classification for lung cancer," *Journal of Thoracic Oncology,* vol. 11, no. 1, pp. 39-51, 2016.

[47] F. C. Detterbeck, "The eighth edition TNM stage classification for lung cancer: What does it mean on main street?," *The Journal of thoracic and cardiovascular surgery,* vol. 155, no. 1, pp. 356-359, 2018.

[48] M. B. Amin *et al.*, "The eighth edition AJCC cancer staging manual: continuing to build a bridge from a population-based to a more "personalized" approach to cancer staging," *CA: a cancer journal for clinicians,* vol. 67, no. 2, pp. 93-99, 2017.